PERGAMON

International Journal of Heat and Mass Transfer 42 (1999) 2955–2965

International Journal of HEAT and MASS TRANSFER

Mixed convection heat and mass transfer in rectangular ducts rotating about a parallel axis

Wei-Mon Yan

Department of Mechanical Engineering, Huafan University, Shih Ting, Taipei 22305, Taiwan, Republic of China

Received 1 May 1998; in final form 25 September 1998

Abstract

A numerical study was performed to examine the characteristics of laminar mixed convection heat and mass transfer in rectangular ducts rotating about a parallel axis with water film evaporation along the porous duct walls. Particular attention is paid to the investigation of the extent of the energy transport through the mass transfer related to film evaporation. Numerical results are presented for an air–water vapor system under various conditions. For a specific condition, a vorticity–velocity method implemented with a marching technique was employed to solve the resultant three-dimensional system for simultaneously developing flow, temperature and concentration fields. Results reveal that the effects of water film vaporization along the porous duct walls on the mixed convection heat and mass transfer are significant. The heat exchange along the porous wetted wall is dominated by the latent heat transport in association with liquid film vaporization. Additionally, the local friction factors and heat and mass transfer rates can be enhanced by the rotational effects, including Coriolis and centrifugal forces, and liquid film evaporation; and the variations of the local values are closely related to the evolution of the secondary vortices in the duct.

Nomenclature

a, b width and height of a rectangular duct, respectively [m]
A cross-sectional area of a rectangular duct [m^2]
D_e equivalent hydraulic diameter, $4A/S$
E dimensionless eccentricity of the rotating ducts, H/D_e
f peripherally averaged friction factor, $2\bar{\tau}_w/(\rho u_0^2)$
g gravitational acceleration
Gr_T rotational heat transfer Grashof number $(\Omega^2 H)\beta(T_w - T_0)D_e^3/v^2$
Gr_M rotational mass transfer Grashof number $(\Omega^2 H)(M_a/M_v - 1)(c_w - c_0)D_e^3/v^2$
h circumferentially averaged heat transfer coefficient [W m^{-2} °C^{-1}]
J rotational Reynolds number, $\Omega D_e^2/v$
$\dot{m}''$ interfacial mass flux due to liquid film evaporation
M, N number of grid points in Y- and Z-directions, respectively
M_a, M_v molecular weights of air and water vapor, respectively
n dimensionless direction coordinate normal to the duct wall
Nu_l local Nusselt number (latent heat)
Nu_s local Nusselt number (sensible heat)
Nu_x overall Nusselt number ($=Nu_l+Nu_s$)
$\bar{p}$ cross-sectional mean pressure [kPa]
p_w partial pressure of water vapor on the wetted walls
$\bar{P}$ dimensionless cross-sectional mean pressure
Pr Prandtl number, v/α
Re Reynolds number, $u_0 D_e/v$
Ro rotational number, $\Omega D_e/u_0$
S circumference of cross-section [m]
S^* parameter, equation (15)
Sc Schmidt number, v/D
Sh local Sherwood number
T temperature [°C]
T_0 inlet temperature [°C]
T_w porous wall temperature [°C]
u, v, w velocity components in x-, y- and z-directions, respectively [m s^{-1}]
u_0 inlet mean velocity [m s^{-1}]
U, V, W dimensionless velocity components in X-, Y- and Z-directions, respectively

* E-mail: wmyan@huafan.hfu.edu.tw

0017–9310/99/$ - see front matter
PII: S0017–9310(98)00350–0

V_i, W_i dimensionless transverse evaporating velocities of the mixture on the wetted walls
x, y, z rectangular coordinate [m]
X^* dimensionless axial coordinate, $X^* = x/(D_e Pr\, Re) = X/Pr$
X, Y, Z dimensionless rectangular coordinate, $X = x/(D_e\, Re)$, $Y = y/D_e$, $Z = z/D_e$.

Greek symbols
α thermal diffusivity [$m^2\ s^{-1}$]
β coefficient of thermal expansion
γ aspect ratio of a rectangular duct, a/b
θ dimensionless temperature $(T-T_0)/(T_w-T_0)$
ν kinematic viscosity [$m^2\ s^{-1}$]
ξ dimensionless vorticity in axial direction
ρ density [kg m^{-3}]
τ_w wall shear stress [kPa]
ϕ relative humidity of moist air in the ambient
Ω angular speed of rotation.

Subscripts
b bulk fluid quantity
0 condition at inlet
w value at wall.

Superscript
$(\bar{\ })$ peripherally-averaged quantity.

1. Introduction

Gas–liquid flow systems with coupled heat and mass transfer are widely encountered in practical applications. Liquid film evaporator, turbine blade cooling, cooling of microelectronic equipment, protection of system components from high temperature gas streams in supersonic aircraft and combustion chambers, and the simultaneous diffusion of metabolic heat and perspiration in the control of our body temperature are just some examples. Because of such widespread applications, latent heat transfer associated with liquid film evaporation in convection heat transfer has received considerable attention.

Developments in rotating machinery have motivated a great deal of research into the effects of rotation on the fluid flow and heat transfer characteristics. Coolant passages are used extensively in rotary machinery where there is a requirement to remove heat to ensure reliable long-term operation. In order to enhance the heat transfer between the walls and the fluid in the duct, the benefit of the film evaporation along the porous duct walls may be considered to augment the heat transfer.

A vast amount of work, both theoretical and experimental, exists in the open literature to examine the flow and heat transfer in rotating ducts. Only those related to the present work are reviewed here. By using a boundary-layer model, Mori and Nakayama [1] and Nakayama [2] investigated laminar and turbulent forced convection heat transfer in a fully-developed flow. Their results were restricted to high rotational speeds. The effects of external convection and tube rotation on the heat transfer in a fully-developed turbulent flow inside an axially rotating tube were examined by Weigand and Beer [3].

Experimental evidence of rotational effects on laminar heat transfer and pressure drop has been reported by Woos [4] and Johnson and Morris [5]. Morris and Dias [6] and Johnson and Morris [7] experimentally investigated the turbulent forced convection heat transfer in the entrance region of a revolving circular and square duct. They found that the increase in the flow resistance due to rotation were typically 30–40% in the laminar flow regime, but 10% in the turbulent regime. Heat transfer and flow in an elliptical duct rotating about a parallel axis was conducted experimentally by Mahadevappa [8]. It was disclosed that, for fully developed laminar and turbulent flows, the increase in heat transfer due to rotation for an elliptical duct lies between the values for circular and square ducts.

Laminar mixed convection heat transfer and fluid flow in developing and fully-developed regions of a circular tube rotating in a parallel mode was numerically studied by Skiadaressis and Spalding [9]. Neti et al. [10] and Levy et al. [11] have numerically and experimentally investigated laminar mixed convection heat transfer in a rotating rectangular duct of aspect ratio $\gamma = 0.5$. In their studies, the centrifugal-buoyancy effects on the flow and heat transfer characteristics were not addressed in detail. The laminar flow in the developing region of an axially rotating pipe was studied numerically by Imao et al. [12] and Gethin and Johnson [13]. Their results indicated that the rotation has a significant impact on the flow field. Mahadevappa et al. [14] analyzed fully developed flow and heat transfer under the influence of rotation-induced buoyancy in rotating rectangular and elliptical ducts. Recently, Soong and Yan [15] numerically investigated the mixed convection heat transfer in rectangular ducts rotating about a parallel axis. It revealed that the rotation-induced buoyancy has a significant effect on the characteristics of flow structure and heat transfer.

As far as convection heat and mass transfer are concerned, evaporation of water film into a gas stream along a flat plate was investigated by Schroppel and Thiele [16] and Chow and Chung [17, 18]. The effects of combined buoyancy forces of heat and mass diffusion on laminar forced convection heat transfer in a vertical parallel-plate channel or pipe were well studied. Santarelli and Foraboschi [19] examined the buoyancy effects on laminar forced convection flow undergoing a chemical reaction. The effects of wetted wall on laminar or turbulent mixed convection heat and mass transfer in vertical ducts were performed by Lin et al. [20] and Yan [21, 22]. In their analyses, they found that the combined buoyancy forces of thermal and mass diffusion have con-

siderable effects on laminar or turbulent forced convection. Mixed convection heat and mass transfer in horizontal or vertical rectangular ducts has been studied by Lin et al. [23] and Lee et al. [24]. In refs. [23, 24], uniform temperature and concentration conditions are assumed along the porous duct walls.

Regardless of its importance in engineering applications, the mixed convection heat and mass transfer in rectangular ducts rotating about a parallel axis has not been well evaluated. This motivates the present investigation.

2. Analysis

Consider the steady and laminar flow through an isothermal rectangular duct rotating at a constant angular speed Ω about an axis parallel to the duct centerline, as shown schematically in Fig. 1. In this work, a moist air with a uniform axial velocity u_0, constant temperature T_0 and relative humidity ϕ enters the duct. The porous duct walls are wetted by a thin liquid film and maintained at a constant temperature T_w. The u, v, and w are the velocity components in the x-, y- and z-directions, respectively. The flow is assumed to be of constant properties except the density variations in the centrifugal terms. The thermophysical properties of the mixture are evaluated by the one-third rule [17]. A detailed calculation of thermophysical properties is available in Fujji et al. [25]. The Boussinesq approximation is invoked for consideration of centrifugal-buoyancy. For a sufficiently fast rotating system, gravitational force is neglected for its small magnitude compared to the centrifugal force. Since no circulation is expected in the primary flow direction (x-direction), the downstream influence on the flow can be ignored. This is justified as the Peclect number Pe is high enough, e.g. $Pe > 100$ [26]. Additionally, the liquid film on the wetted porous wall is assumed to be extremely thin and it can be treated as a boundary condition.

Based on the above assumptions, the problem can be described by the following dimensionless vorticity–velocity formulation:

$$\partial^2 V/\partial Y^2 + \partial^2 V/\partial Z^2 = -\partial\xi/\partial Z - \partial^2 U/\partial X\,\partial Y \tag{1}$$

$$\partial^2 W/\partial Y^2 + \partial^2 W/\partial Z^2 = \partial\xi/\partial Y - \partial^2 U/\partial X\,\partial Z \tag{2}$$

$$\begin{aligned} &U\partial\xi/\partial X + V\partial\xi/\partial Y + W\partial\xi/\partial Z + \xi\,\partial U/\partial X \\ &\quad + (\partial U/\partial Y\cdot\partial W/\partial X - \partial U/\partial Z\cdot\partial V/\partial X) \\ &\quad = (\partial^2\xi/\partial Y^2 + \partial^2\xi/\partial Z^2) - 2J\,\partial U/\partial X \\ &\quad + [Y/E + 1 - (1+\gamma)/(4\gamma E)]\cdot(Gr_T\,\partial\theta/\partial Z \\ &\quad + Gr_M\,\partial C/\partial Z) - [Z/E - (1+\gamma)/(4E)] \\ &\quad \cdot(Gr_T\,\partial\theta/\partial Y + Gr_M\,\partial C/\partial Y) \end{aligned} \tag{3}$$

$$\begin{aligned} &U\,\partial U/\partial X + V\,\partial U/\partial Y + W\,\partial U/\partial Z \\ &\qquad = -\mathrm{d}\bar{P}/\mathrm{d}X + \partial^2 U/\partial Y^2 + \partial^2 U/\partial Z^2 \end{aligned} \tag{4}$$

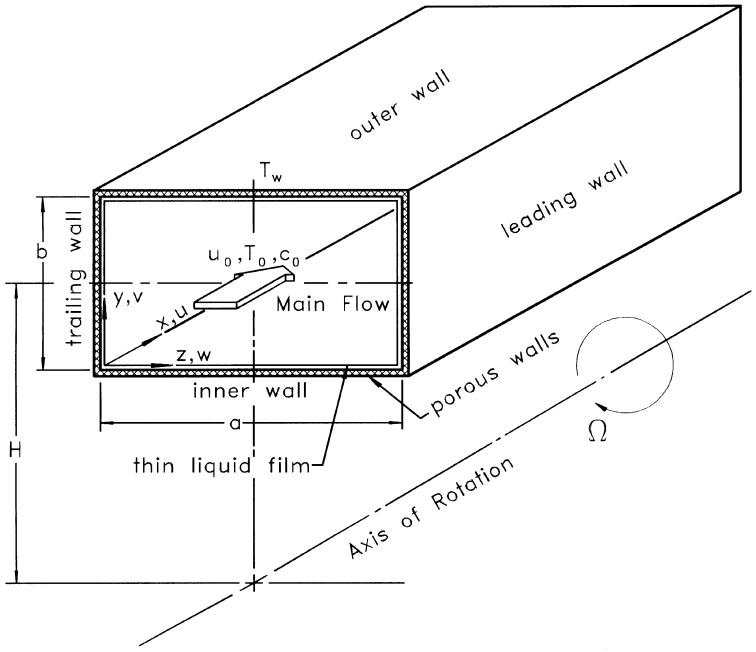

Fig. 1. Schematic diagram of the physical system.

$$U\partial\theta/\partial X+V\partial\theta/\partial Y+W\partial\theta/\partial Z=(\partial^2\theta/\partial Y^2+\partial^2\theta/\partial Z^2)/Pr \quad (5)$$

$$U\partial C/\partial X+V\partial C/\partial Y+W\partial C/\partial Z=(\partial^2 C/\partial Y^2+\partial^2 C/\partial Z^2)/Sc \quad (6)$$

where the dimensionless variables and groups are defined as follows.

$$X=x/(D_e\,Re)\quad Y=y/D_e$$
$$Z=z/D_e\quad U=u/u_0$$
$$V=vD_e/v\quad W=wD_e/v$$
$$\bar{P}=\bar{p}/(\rho u_0^2)\quad X^*=X/Pr$$
$$\theta=(T-T_0)/(T_w-T_0)\quad C=(c-c_0)/(c_w-c_0)$$
$$Re=u_0D_e/v\quad Pr=v/\alpha$$
$$Gr_T=(\Omega^2D_e)\beta(T_w-T_0)D_e^3/v^2$$
$$Gr_M=(\Omega^2D_e)(M_a/M_v-1)(c_w-c_0)D_e^3/v^2$$
$$J=\Omega D_e^2/v\quad E=H/D_e$$
$$\gamma=a/b\quad D_e=4A/S. \quad (7)$$

For proper calculation of the axial pressure gradient, $-\mathrm{d}\bar{P}/\mathrm{d}X$, the global mass conservation,

$$\int_0^{(1+\gamma)/(2\gamma)}\int_0^{(1+\gamma)/2}U\,\mathrm{d}Y\,\mathrm{d}Z=(1+\gamma)^2/(4\gamma)+\int_0^X\int_0^{(1+\gamma)/2}(V_1-V_2)\,\mathrm{d}Z\,\mathrm{d}X+\int_0^X\int_0^{(1+\gamma)/(2\gamma)}(W_1-W_2)\,\mathrm{d}Y\,\mathrm{d}X \quad (8)$$

has to be satisfied at each axial location. The present problem is subjected to the following boundary conditions:

$$U=W=0,\quad V=V_1,\quad \theta=C=1\quad \text{at } Y=0 \quad (9a)$$
$$U=W=0,\quad V=V_2,\quad \theta=C=1\quad \text{at } Y=(1+\gamma)/(2\gamma) \quad (9b)$$
$$U=V=0,\quad W=W_1,\quad \theta=C=1\quad \text{at } Z=0 \quad (9c)$$
$$U=V=0,\quad W=W_2,\quad \theta=C=1\quad \text{at } Z=(1+\gamma)/2 \quad (9d)$$
$$U=1,\quad V=W=\xi=\theta=0\quad \text{at the entrance } X=0. \quad (9e)$$

Since the air–water interface is semipermeable (the solubility of air in water is negligibly small) and air velocity in the direction normal to the wetted wall is stationary at the interface, the evaporating velocities of the mixture on the wetted surfaces are evaluated by the following equations [27]

$$V_i=-(c_w-c_0)\cdot(\partial C/\partial Y)/[Sc(1-c_w)],\quad i=1,2 \quad (10a)$$
$$W_i=-(c_w-c_0)\cdot(\partial C/\partial Z)/[Sc(1-c_w)],\quad i=1,2 \quad (10b)$$

where the subscript $i=1$ represents the wall of $Y=0$ or $Z=0$, while $i=2$ indicates the condition at the wall of $Y=(1+\gamma)/(2\gamma)$ or $Z=(1+\gamma)/2$. According to Dalton's law and the state equation of ideal gas mixture, the interface mass fraction of water vapor can be calculated by

$$c_w=p_wM_v/[p_wM_v+(p-p_w)M_a] \quad (11)$$

where p_w is the partial pressure of water vapor on the wetted wall.

After the developing velocity, temperature and concentration fields being obtained, the computations of the circumferentially averaged friction factor, Nusselt and Sherwood numbers are of practical interest. Following the usual definitions, the expression for the product of the peripherally averaged friction factor and Reynolds number fRe can be written as

$$fRe=-2(\overline{\partial U/\partial n})_w. \quad (12)$$

Energy transport between the wetted walls and the fluid in the duct in the presence of mass transfer depends on two factors: (1) the fluid temperature gradient at the porous duct walls, resulting in a sensible heat transfer, and (2) the rate of mass transfer, resulting in a latent heat transfer. The local Nusselt numbers along the channel can then be written as [20, 24]

$$Nu_x=Nu_s+Nu_l \quad (13)$$

where Nu_s and Nu_l are, respectively, the local Nusselt numbers for sensible and latent heat transfer, they are defined as

$$Nu_s=(\overline{\partial\theta/\partial n})_w/(1-\theta_b) \quad (14a)$$
$$Nu_l=S^*(\overline{\partial C/\partial n})_w/[(1-c_w)\cdot(1-\theta_b)]=h_{fg}/[c_p(T_w-T_b)]\cdot(c_w-c_b)/(1-c_w)\cdot(Pr/Sc)\cdot Sh \quad (14b)$$

where S^* indicates the importance of the energy transport through species diffusion relative to that through thermal diffusion

$$S^*=\rho Dh_{fg}(c_w-c_0)/[k(T_w-T_0)]. \quad (15)$$

Similarly, the local Sherwood number Sh is defined as

$$Sh=(\overline{\partial C/\partial n})_w/(1-C_b) \quad (16)$$

where the overbar means the average around the perimeters and n denotes the dimensionless coordinate normal to the porous duct walls. The bulk fluid temperature θ_b and bulk fluid concentration C_b are defined as

$$\theta_b=\int_0^{(1+\gamma)/(2\gamma)}\int_0^{(1+\gamma)/2}\theta\cdot U\,\mathrm{d}Y\,\mathrm{d}Z\Big/\int_0^{(1+\gamma)/(2\gamma)}\int_0^{(1+\gamma)/2}U\,\mathrm{d}Y\,\mathrm{d}Z \quad (17)$$

$$C_b=\int_0^{(1+\gamma)/(2\gamma)}\int_0^{(1+\gamma)/2}C\cdot U\,\mathrm{d}Y\,\mathrm{d}Z\Big/\int_0^{(1+\gamma)/(2\gamma)}\int_0^{(1+\gamma)/2}U\,\mathrm{d}Y\,\mathrm{d}Z. \quad (18)$$

The parameters involved in the present problem are the Prandtl number Pr, Schmidt number Sc, rotational Reynolds number J, heat transfer Grashof number Gr_T, mass transfer Grashof number Gr_M, eccentricity E and cross-sectional aspect ratio γ. The rotational Reynolds number J characterizes the Coriolis force effect or a measure of the relative strength of Coriolis force to viscous force. The Gr_T and Gr_M measure the significance of the rotation-induced buoyancy effects. It should be mentioned herein that not all the values of nondimensional groups can be arbitrarily assigned. Some of them (i.e. Pr, Sc, Gr_T, Gr_M, and J) are interdependent for a given mist air under certain specific conditions. Hence, for a given mixture it is not proper to vary Pr, Sc, Gr_T or Gr_M independently in order to study their individual effects. Instead the physical parameters—wall temperature T_w, relative humidity of the ambient moist air ϕ and rotational speed Ω are chosen as the independent variables. In light of practical situations, the following conditions are selected in the computations: unsaturated moist air at the inlet is fixed at 20°C and 1 atm, the relative humidity of inlet mixture ϕ is chosen to be 10, 50 or 90%, the wetted walls are maintained at a constant wall temperature of 40, 60 and 80°C, and the angular speed Ω is chosen to be 400, 800 or 1200 rpm. Based on the specific conditions, the dimensionless groups can then be obtained for several cases, as indicated in Table 1.

3. Solution method

The governing equations are solved by the vorticity–velocity method for three-dimensional parabolic flow [28]. For a given condition, the field solutions are calculated by a marching technique based on the Du Fort–Frankel scheme [28]. Details of the solution procedure has been described elsewhere [15, 24], and is not repeated herein.

To obtain enhanced accuracy, grids were chosen to be uniform in the cross-sectional direction but nonuniform in the axial direction to account for the uneven variations of velocity, temperature and concentration in the entrance region. It was found in Table 2 that the deviations in local Nu_x calculated with $M \times N = 51 \times 51$ and 71×71 ($\Delta X^* = 1 \times 10^{-5}$–$2 \times 10^{-4}$) are always less than 1% for a typical case. Furthermore, the deviations in local Nu_x calculated using $M \times N(\Delta X^*) = 51 \times 51$ (1×10^{-6}–2×10^{-4}) and 51×51 (1×10^{-5}–2×10^{-4}) are all less than 1%. Accordingly, the computations involving a $M \times N(\Delta X^*) = 51 \times 51$ (1×10^{-5}–2×10^{-4}) grid are considered to be sufficiently accurate to describe the mixed convection heat and mass transfer in rectangular duct rotating about a parallel axis. All the results presented in the next section are computed using the latter grid. As a partial verification of the computational procedure, results were initially obtained for mixed convection heat transfer in rotating rectangular duct of aspect ratio $\gamma = 0.5$ without mass transfer. The present predictions of peripheral average of Nu in an iso-flux duct of $\gamma = 0.5$ are compared with the computation and measurement by Neti et al. [10] and Levy et al. [11]. It is found that the results agree well with both the computations and measured data of Levy's group for $Gr_T < 1 \times 10^6$. Generally speaking, the methodology employed gives very reasonable predictions of the limiting case. The above numerical tests indicated that the solution procedure adopted is suitable for the present study.

4. Results and discussion

Figure 2 depicts a series of cross-flow velocity distributions in the transverse plane at different axial locations. Each of the velocity vectors in the cross-flow plane is composed of the velocity components in the y- and z-directions. Near the entrance ($X^* = 0.0004$), the flow is of boundary-layer type, the fluid is repelled from the near-wall region toward the center of the duct for the boundary layer displacement effect. As the flow moves downstream ($X^* = 0.02$), the cross flow shows a spiral pattern with a tendency of vortex formation. A stronger

Table 1
Parameters and conditions used in this work for different aspect ratio γ

Case	Ω (rpm)	T_w (°C)	ϕ (%)	Gr_T	Gr_M	J	Pr	Sc
I	800	40	50	1.83×10^4	6.44×10^3	518.48	0.703	0.592
II	800	60	50	3.24×10^4	1.80×10^4	487.04	0.701	0.582
III	800	80	50	4.44×10^4	4.57×10^4	465.73	0.716	0.565
IV	1200	40	50	4.13×10^4	1.45×10^4	777.72	0.703	0.592
V	400	40	50	4.58×10^3	1.61×10^3	259.24	0.703	0.592
VI	800	40	10	1.82×10^4	7.37×10^3	518.20	0.703	0.592
VII	800	40	90	1.84×10^4	5.49×10^3	518.77	0.703	0.591

Table 2
Comparisons of local Nu_x for various grid arrangements for $\Omega = 800$ rpm, $T_w = 40^\circ C$, $\phi = 50\%$ and $\gamma = 1$

$M \times N$ (ΔX^*)	X^*					
	0.001	0.005	0.01	0.05	0.1	0.3
51×51 (1×10^{-5}–2×10^{-4})	77.70	38.45	30.28	29.66	20.62	11.61
71×71 (1×10^{-5}–2×10^{-4})	76.26	38.37	30.29	29.67	20.54	11.60
51×51 (1×10^{-6}–2×10^{-4})	77.98	38.51	30.29	29.67	20.60	11.61
31×31 (1×10^{-5}–2×10^{-4})	86.98	38.96	30.46	29.92	20.89	11.61

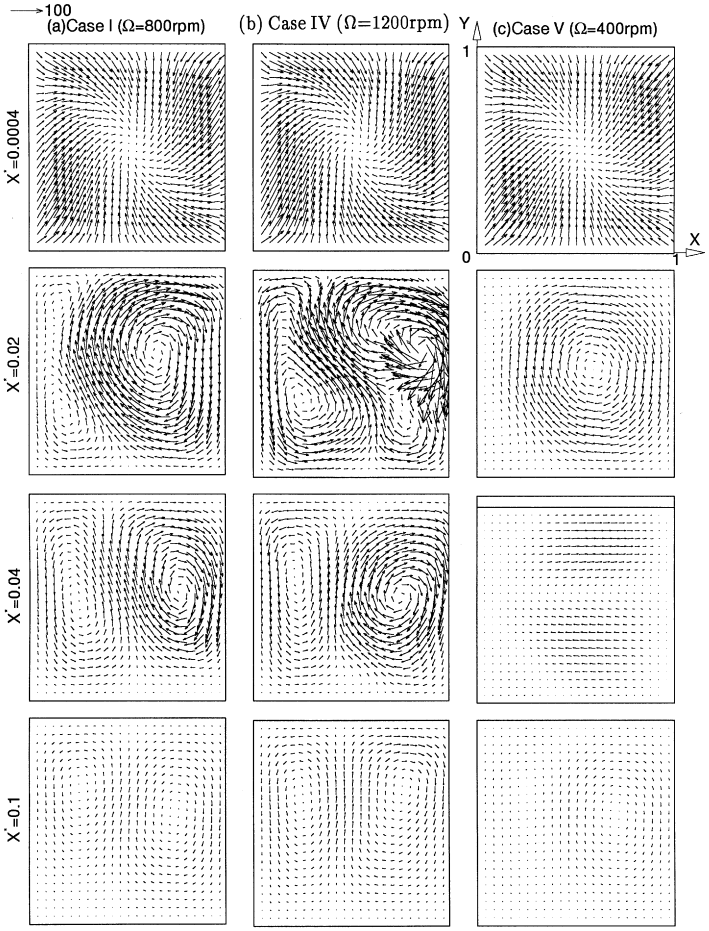

Fig. 2. Effects of angular speed Ω on the cross-flow velocity distributions ($\gamma = 1$).

secondary flow is noted for a system with a higher rotation speed (case IV, $\Omega = 1200$ rpm). Additionally, the flow pattern is more twisted for a higher rotation speed (case IV, $\Omega = 1200$ rpm) and therefore has more potential for formation of the secondary vortices. But for the case of lower rotation speed (case V, $\Omega = 400$ rpm), a weaker vortex is found due to a weaker Coriolis effect. Further downstream ($X^* = 0.1$), the vortices become weak. In the separate numerical runs, the secondary motion would fade away in the far downstream as the flow field approaches the fully-developed condition.

To investigate the relative contributions of heat transfer through sensible and latent heat transfer, the local Nusselt number distributions are shown in Fig. 3 with

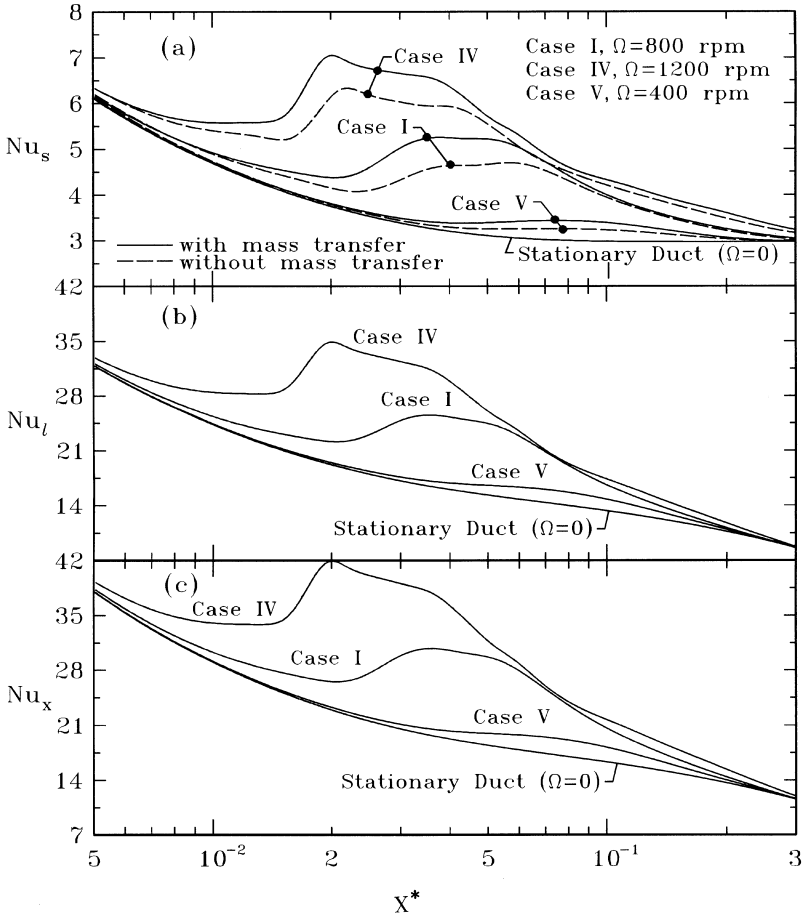

Fig. 3. Effects of angular speed Ω on the local Nusselt numbers ($\gamma = 1$).

angular speed Ω as a parameter. For comparison purposes, the corresponding results without mass transfer are also included in this plot by the dashed curves. An overall inspection of Fig. 3 discloses that the decreases in local values of Nusselt number Nu_s near the inlet are attributed to the forced-convection entrance effect. Proceeding downstream, the Nusselt number Nu_s deviates from that of forced convection ($\Omega = 0$) and decreases monotonically to a local minimum value. At this position, the entrance and rotational effects are balanced out. Location of the local minimum in Nu_s-curve denotes the formation of the secondary vortices and the position of the local minimum Nu_s depending upon the value of Ω. Subsequently, the rotational effects dominate over the entrance effect and the Nu_s increases until a local maximum value of Nu_s is reached. Finally, the curves of Nu_s fall asymptotically to the value of forced convection when the velocity, temperature and concentration fields approach the fully developed condition. Also noted in Fig. 3(a) is that, relative to the results without mass diffusion effects, those with mass transfer effects have a pronounced impact on the local Nu_s for a system with a high angular speed Ω. It was found that in the separate numerical runs that as $\Omega < 200$ rpm, the effects of Ω on the Nu_s are relatively small. By comparing the ordinates in Fig. 3(a) and 3(b), it is observed that the magnitude of Nu_l is much larger than that of Nu_s, indicating that the interfacial heat transfer resulting from latent heat exchange is much more effective. In Fig. 3(c), Nu_x, the sum of Nu_s and Nu_l, is presented.

The effects of angular speed Ω on the local friction factor fRe and Sherwood number Sh are presented in Fig. 4. The local fRe with mass transfer effects is always larger than that without mass transfer effects. This is due to the additional centrifugal mass buoyancy owing to the mass transfer. Additionally, the result with a higher angular speed Ω shows a greater fRe due to the greater rotational effects including Coriolis force and centrifugal

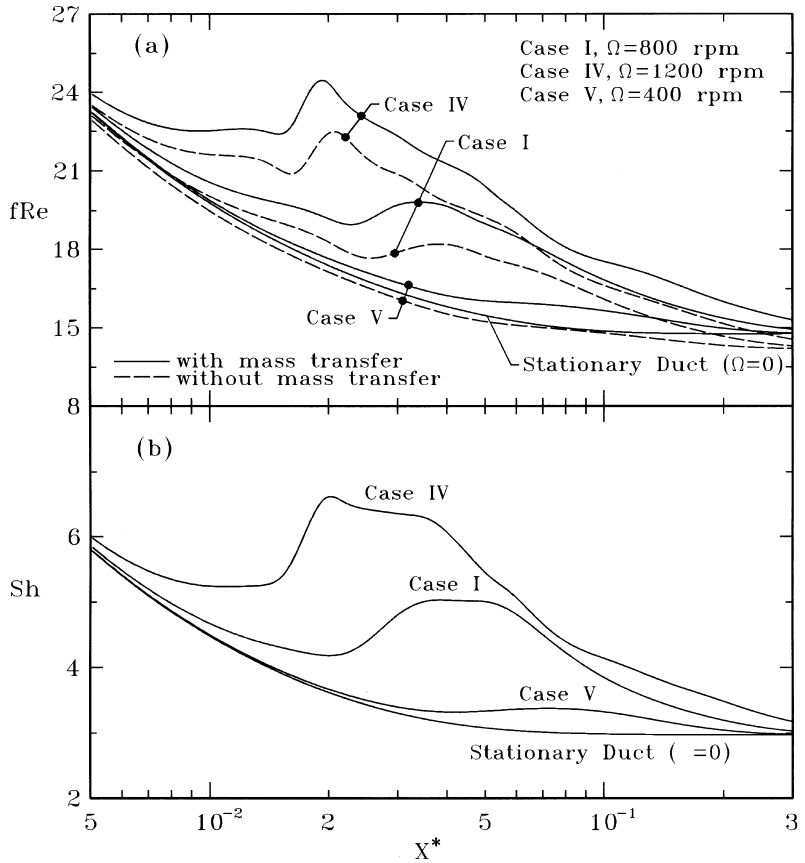

Fig. 4. Effects of angular speed Ω on the local friction factor fRe and Sherwood number Sh ($\gamma = 1$).

buoyancy. In Fig. 4(b), the distributions of Sh resemble those of Nu_s in Fig. 3(a). This is because in this study the Prandtl number Pr and Schmidt number Sc are of the same order of magnitude. Again, a larger Sh is found for the system with a higher Ω.

The effects of porous wall temperature T_w on the local Nusselt number distributions are shown in Fig. 5. Regarding Nu_s curves, a lager Nu_s is noted for a higher T_w due to a greater centrifugal buoyancy effect. Additionally, the heat transfer enhancement due to the mass transfer effects, which can be identified by the vertical separation between the solid curves and dashed curves, increases with the increase in T_w. In Fig. 5(b), the flow with a higher T_w shows a larger Nu_l. This is brought about by the larger latent heat transport in connection with the larger liquid film evaporation for a higher T_w. It is apparent by comparing Fig. 5(a) and 5(b) that, for $T_w = 80°C$, the magnitude of the evaporative latent heat Nusselt number Nu_l may be 15 times greater than that of sensible heat Nusselt number Nu_s. This implies that the heat transfer enhancement due to film evaporation is much more effective for a system with a higher wall temperature T_w.

It is interesting to examine the effects of the relative humidity of the ambient moist air ϕ on the heat exchange of latent heat. The distributions of Nu_l with various values of ϕ are presented in Fig. 6. It is found in the separate computational runs that the influences of ϕ on the developments of velocity, temperature and concentration are rather insignificant. But the influences of ϕ on the latent heat exchange cannot be neglected. A larger Nu_l is found for a system with a lower ϕ. This is owing to the fact that the latent heat exchange associated with film evaporation is much more effective at lower concentration levels.

The effects of the channel aspect ratio γ on the local Nu_x, fRe and Sh are of interest. The axial distributions of Nu_x, fRe and Sh for $\gamma = 0.5$ and 2 are presented in Fig. 7 with angular speed Ω as a parameter. For comparison purposes, the results for $\gamma = 1$ are also included in this figure. Comparing the results with different γ indicates that, within the range of the aspect ratio under consideration, the effects of the aspect ratio on the Nu_x, fRe and Sh are more pronounced for a system with a higher rotation speed. Additionally, for a higher rotation case (case IV), the effects of the angular speed on the Nu_x, fRe and Sh are more significant for square duct ($\gamma = 1$)

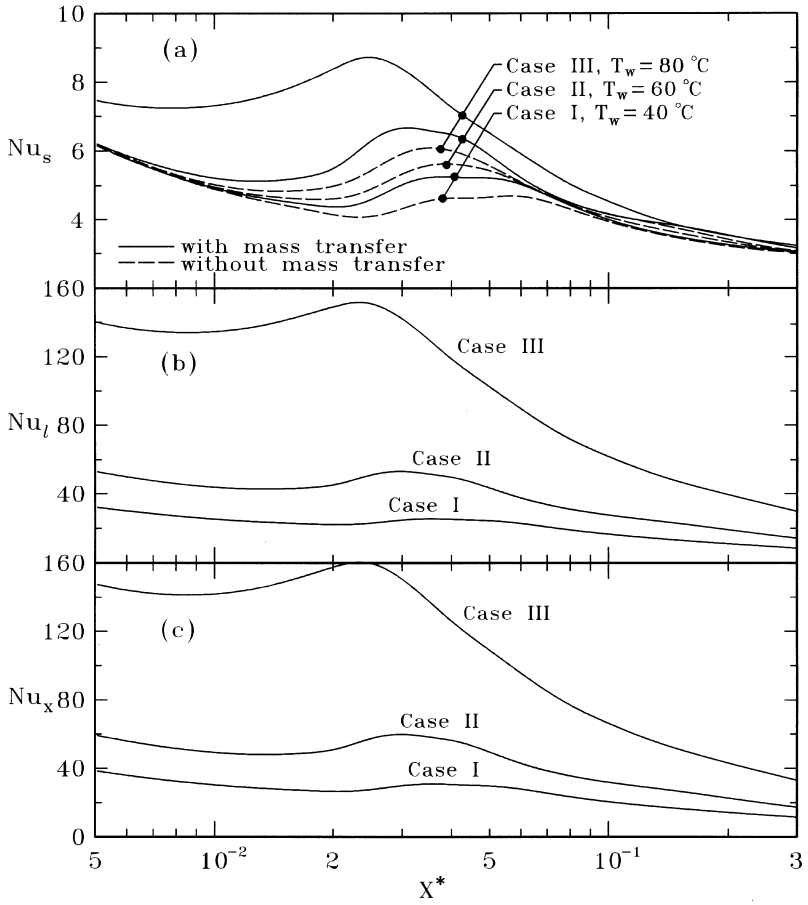

Fig. 5. Effects of wall temperature T_w on the local Nusselt numbers ($\gamma = 1$).

at the range of $X^* = 0.01$–0.05. This is owing to the relatively stronger secondary motion presented for aspect ratio $\gamma = 1$, which in turn causes a larger augmentation in Nu_x, fRe and Sh. As the flow moves downstream, the rotation effect diminishes and the flow approaches a fully-developed condition. Therefore, the values of Nu_s, fRe and Sh at higher value of X^* would approach the limiting results of fully-developed convection heat and mass transfer. As shown in ref. [30], the fully-developed results of Nu (Sh) and fRe in rectangular ducts depends on aspect ratio γ. For $\gamma = 1$, the fully-developed results of Nu (Sh) and fRe are 2.98 and 14.23, respectively. But, for $\gamma = 0.5$ ($\gamma = 2$), the values are 3.39 and 15.56, respectively. From the above stations, these explain why the values of fRe and Sh at higher values of X^* for $\gamma = 0.5$ (or $\gamma = 2$) are different from those of $\gamma = 1$.

5. Conclusions

The effects of mass diffusion on mixed convection flow and heat transfer in rectangular ducts rotating about a parallel axis have been studied numerically. The effects of angular speed Ω, porous wall temperature T_w, the relative humidity of the moist air ϕ and the aspect ratio of the duct γ on the transfer of momentum, heat and mass in the flow were examined in detail. What follows is a brief summary.

(1) Heat transfer on the porous wetted duct walls is dominated by the transport of latent heat in connection with the vaporization of the liquid film.
(2) The variations of the friction factor fRe, Nusselt numbers Nu and Sherwood number Sh show that the total rotational effects of Coriolis and centrifugal buoyancy forces are negligible up to a certain entry length depending primarily on the magnitude of the rotational speed Ω. The distributions of fRe, Nu and Sh are characterized by a decay near the entrance due to the entrance effect; but the decay is attenuated by the onset of secondary flow.
(3) The circumferentially averaged friction factor fRe, Nusselt numbers Nu and Sherwood number Sh are enhanced with an increase in the angular speed Ω and the porous wall temperature T_w.

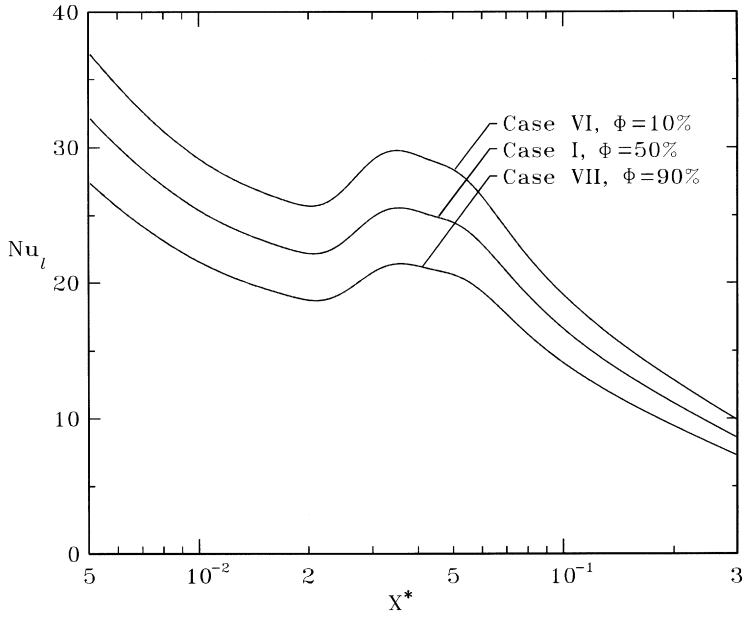

Fig. 6. Effects of relative humidity ϕ on the local Nu_l ($\Omega = 800$ rpm, $\gamma = 1$).

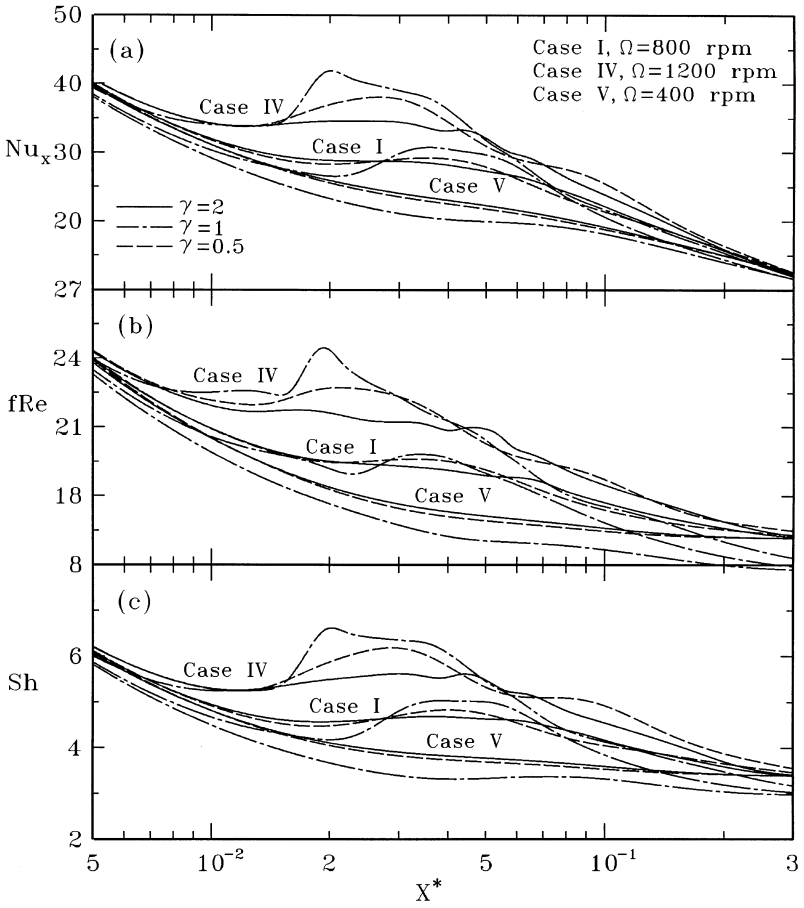

Fig. 7. Effects of aspect ratio γ on the local Nu_x, fRe and Sh.

(4) The centrifugal buoyancy induced by mass diffusion causes an enhancement in heat and mass transfer. The extent of the augmentation increases with an increase in T_w, comparable with the corresponding results without mass transfer.
(5) Greater aspect ratio effects are noted for a system with a higher angular speed.

Acknowledgement

The financial support of this research by the National Science Council, R.O.C., under the contract NSC 86-2212-E-211-007 is greatly appreciated.

References

[1] Y. Mori, W. Nakayama, Forced convection heat transfer in straight pipe rotating around a parallel axis (1st report, laminar region), Int. J. Heat Mass Transfer 10 (1967) 1179–1194.
[2] W. Nakayama, Forced convective heat transfer in a straight pipe rotating around a parallel axis (2nd report, turbulent region), Int. J. Heat Mass Transfer 11 (1968) 1185–1201.
[3] B. Weigand, H. Beer, Fluid flow and heat transfer in an axially rotating pipe subjected to external convection, Int. J. Heat Mass Transfer 35 (1992) 1803–1809.
[4] J.L. Woods, Heat transfer and flow resistance in a rotating duct system. Ph.D. Dissertation, University of Sussex, Falmer, U.K., 1975.
[5] A.R. Johnson, W.D. Morris, Pressure loss measurement in circular ducts which rotate about a parallel axis, Proc. XIV ICHMT Symp. in Rotating Machinery, Dubrovnick, Yugoslavia, Hemisphere, Washington, U.S.A., 1982, pp. 51–62.
[6] W.D. Morris, F.M. Dias, Turbulent heat transfer in a revolving square-sectioned tube, J. Mech. Engrg Sci. 22 (1980) 95–101.
[7] A.R. Johnson, W.D. Morris, An experimental investigation into the effects of rotation on the isothermal flow resistance in circular tubes rotating about a parallel axis, Int. J. Heat Mass Transfer 13 (1992) 132–140.
[8] M. Mahadeveppa, K.V.C. Rao, V.M.K. Sastri, Experimental investigation for fluid flow and heat transfer in an elliptical duct rotating about a parallel axis, Experimental Heat Transfer 6 (1993) 97–109.
[9] D. Skiadaressis, D.B. Spalding, Laminar heat transfer in a pipe rotating around a parallel axis, HRS/76123, Mech. Eng. Dept., Imperial College of Science and Technology, London, U.K., 1976.
[10] S. Neti, A.S. Warnork, E.K. Levy, K.S. Kannan, Computation of laminar heat transfer in rotating rectangular ducts, ASME J. Heat Transfer 107 (1985) 575–582.
[11] E. Levy, S. Neti, G. Brown, F. Bayat, Laminar heat transfer and pressure drop in a rectangular duct rotating about a parallel axis, ASME J. Heat Transfer 108 (1986) 350–356.
[12] S. Imao, Q. Zhang, Y. Yamada, The laminar flow in the developing region of a rotating pipe, JSME Int. J., Series II 32 (1989) 317–323.
[13] D.T. Gethin, A.R. Johnson, Numerical analysis of the developing fluid flow in a circular duct rotating steadily about a parallel axis, Int. J. Numer. Method in Fluids 9 (1989) 151–165.
[14] M. Mahadevappa, K.V.C. Rao, V.M.K. Sastri, Numerical study of laminar fully developed fluid flow and heat transfer in rectangular and elliptical ducts rotating about a parallel axis, Int. J. Heat Mass Transfer 39 (1996) 867–875.
[15] C.Y. Soong, W.M. Yan, Laminar mixed convection flow and heat transfer in entrance region of rectangular ducts rotating about a parallel axis, Proc. of the ASME Heat Transfer Division, HTD-Vol. 317-1 (1995) 373–384.
[16] J. Schroppel, F. Thiele, On the calculation of momentum, heat and mass transfer in laminar and turbulent boundary layer flow along a vaporizing liquid film, Numer. Heat Transfer 6 (1983) 475–496.
[17] L.C. Chow, J.N. Chung, Evaporation of water into a laminar stream of air and superheated steam, Int. J. Heat Mass Transfer 26 (1983) 373–380.
[18] L.C. Chow, J.N. Chung, Water evaporation into a turbulent stream of air, humid air or superheated steam, 21st ASME/AIChE National Heat Transfer Conference, Seattle, WA, ASME paper No. 83-HT-2, 1983.
[19] F. Santarelli, F.P. Foraboschi, Heat transfer in laminar mixed convection in a reacting fluid, Chem. Eng. 6 (1973) 59–68.
[20] T.F. Lin, C.J. Chang, W.M. Yan, Analysis of combined buoyancy effects of thermal and mass diffusion on laminar forced convection heat transfer in a vertical tube, ASME J. Heat Transfer 110 (1988) 337–344.
[21] W.M. Yan, Turbulent mixed convection heat and mass transfer in a wetted channel, ASME J. Heat Transfer 117 (1995) 229–233.
[22] W.M. Yan, Effects on film vaporization on turbulent mixed convection heat and mass transfer in a vertical channel, Int. J. Heat Mass Transfer 38 (1995) 713–722.
[23] J.N. Lin, F.C. Chou, W.M. Yan, P.Y. Tzeng, Combined buoyancy effects of thermal and mass diffusion on laminar forced convection in the thermal entrance region of horizontal square channels, Can. J. Chem. Eng. 79 (1992) 681–689.
[24] K.T. Lee, H.L. Tsai, W.M. Yan, Mixed convection heat and mass transfer in verticular rectangular ducts, Int. J. Heat Mass Transfer 40 (1997) 1621–1631.
[25] T. Fujji, Y. Kato, K. Mihara, Expression of transport and thermodynamic properties of air, steam and water, Sei San Ka Gaku Ken Kyu Jo., Report No. 66, Kyu Shu Dai Kaku, Kyu Shu, Japan, 1978, pp. 81–95.
[26] R.A. Shah, A.L. London, Laminar flow forced convection in ducts, Adv. Heat Transfer Suppl. 1 (1978) 196–222.
[27] E.R.G. Eckert, R.M. Drake Jr., Analysis of Heat and Mass Transfer, Chaps 20 and 22, McGraw-Hill, New York, 1972.
[28] K. Ramakrishna, S.G. Rubin, P.K. Khosla, Laminar natural convection along vertical square ducts. Numer. Heat Transfer 5 (1982) 59–79.
[29] P.J. Roche, Computational Fluid Dynamics. Reinhold, New York, 1971, pp. 61–64.
[30] S. Kakac, R.K. Shah, W. Aung, Handbook of Single-Phase Convective Heat Transfer, John Wiley and Sons, 1987, pp. 3–46.